



**HAL**  
open science

## Origin of an intermediate peak in DMTA analysis of multilayer ABS/PC samples

Aboubaker Alkhuder, Anne-sophie Caro, Matthieu Gervais, Alain Guinault, Patrick Ienny, Perrin Didier, Cyrille Sollogoub

### ► To cite this version:

Aboubaker Alkhuder, Anne-sophie Caro, Matthieu Gervais, Alain Guinault, Patrick Ienny, et al.. Origin of an intermediate peak in DMTA analysis of multilayer ABS/PC samples. *Journal of Applied Polymer Science*, 2024, 141 (6), pp.e54926. 10.1002/app.54926 . hal-04426974

**HAL Id: hal-04426974**

**<https://hal.science/hal-04426974>**

Submitted on 30 Jan 2024

**HAL** is a multi-disciplinary open access archive for the deposit and dissemination of scientific research documents, whether they are published or not. The documents may come from teaching and research institutions in France or abroad, or from public or private research centers.

L'archive ouverte pluridisciplinaire **HAL**, est destinée au dépôt et à la diffusion de documents scientifiques de niveau recherche, publiés ou non, émanant des établissements d'enseignement et de recherche français ou étrangers, des laboratoires publics ou privés.

# Origin of an intermediate peak in DMTA analysis of multilayer ABS/PC samples

A. Alkhuder<sup>1</sup>, A.S. Caro<sup>2</sup>, M. Gervais<sup>3</sup>, A. Guinault<sup>3</sup>, P. Jenny<sup>2</sup>, D. Perrin<sup>4</sup>, C. Sollogoub<sup>3</sup>

<sup>1</sup> P-2AM, CNAM, 292, rue Saint-Martin, 75003 Paris, France

<sup>2</sup> LMGC, IMT Mines Ales, Université Montpellier, CNRS, 30100 Ales, France

<sup>3</sup> PIMM – UMR 8006, ENSAM, CNRS, CNAM, 151 bd de l'Hôpital, 75013 Paris, France

<sup>4</sup> Polymers Composites and Hybrids (PCH), IMT Mines Ales, 30100 Ales, France

## Keywords

Viscoelasticity; Damping; Finite element method; ABS/PC blends; Interphase

## Abstract

Three layers film shaped by thermocompression of ABS and PC have been analyzed in dynamic mechanical thermal analysis in tensile mode. They present two peaks as the film is loaded perpendicularly to the layers and three peaks as the film is loaded in parallel to the layers. Numerical computations confirm that the origin of this peak is not related to a mechanical issue such as the transmission of the imposed deformation from one layer to the other. Using this method, it is demonstrated that this third peak can only be obtained assuming a material transition with its own behavior between layers.  $\tan \delta$  measurements provide a simple and useful experimental tool to understand more about the interfacial zone in polymer blends.

## Introduction

Multiphase polymer materials (nanocomposites, polymer blends, copolymers, interpenetrating polymer networks, particulate filled polymers) have emerged as a new class of materials with enhanced properties that may be tailored to meet increasingly stringent specifications<sup>1</sup>. The properties of such systems depend not only on the properties of the individual components, their composition and morphology, but also on the chemical and physical interactions between the different phases<sup>2</sup>. In particular, the existence of an interphase, a more or less extensive area of interdiffusion or adsorption between the different components, with its own characteristic properties or property gradients, has been shown to affect the final properties of the systems: mechanical properties<sup>3-5</sup>, thermal transport<sup>6</sup>, gas barrier properties<sup>7</sup>, ageing and degradation<sup>8</sup>. Due to its small size, the interphase is quite difficult to characterize and finding a relevant tool to study its extent and properties remains still a challenge. Among the various experimental techniques used to characterize interphases (direct imaging by microscopic techniques<sup>9,10</sup>, reflectometry techniques either with X-rays or neutrons<sup>11</sup>), Dynamic Thermomechanical Analysis (DMTA) has been proven to be an excellent probe, highly sensitive and able to give insight on the viscoelastic properties and the various relaxational mechanisms in the global systems<sup>12-14</sup>. In most cases, an additional damping peak was observed for multiphase polymer systems and correlated with an interphase region<sup>15-17</sup>. The origin of this additional peak, observed in DMTA spectra but not revealed by Differential Scanning Calorimetry (DSC), has

been widely discussed in the literature<sup>18,19</sup> and several explanations have been proposed: specific molecular relaxation process in the interfacial region, change in the relative moduli values of the components in the matrix-interphase-particle structure of the blend, layer with different mechanical properties resulting from the residual thermal stresses.

An additional damping peak, located at a temperature between the glass transitions of the two components, has in particular been observed in multilayered polymer system<sup>20-24</sup>. While for some authors, the origin of this intermediate peak is purely mechanical, just reflecting the additive effect of the damping behavior of each phase, some others point out the importance of interfacial stress due to different thermal expansion between layers. Many efforts have been done to investigate the impact on the occurrence and amplitude of the third peak of several experimental parameters: composition ratio, number of layers, chain orientation, residual stress, cyclic, etc. Some contradictory results suggested that the influential parameters are highly dependent on the system studied, in particular on the compatibility between the two combined polymers, i.e. the presence of an interphase, namely an interfacial layer. For example, while for polycarbonate/poly(styrene-co-acrylonitrile) (PC/SAN) multilayered systems the peak is insensitive to the number of layers<sup>20</sup>, its intensity is increased as the number of layers increases for more compatible systems like polypropylene/polyolefin elastomer (PP/POE)<sup>24</sup>, propylene-ethylene copolymer/polyolefin elastomer (PPE/POE)<sup>25</sup> or poly(vinyl chloride)/chlorinated butyl rubber (PVC/CIIR)<sup>26</sup> system. Some other parameters may have an effect on the presence of the third peak such as the difference between the glass transition temperatures of the two polymers, the difference between their moduli and their temperature dependence or the coefficient of thermal expansion of both polymers. As shown by Shen et al.<sup>25</sup>, a two-component Takayanagi model<sup>27</sup> is unable to predict the apparition of the third peak suggesting that a more complete simulation is needed. Zhang et al.<sup>28</sup> performed a finite element analysis to simulate the distribution of shear strain in the alternating multilayer system but did not simulate the temperature dependence of the loss factor.

In this study, we aim at gaining insights on the origin of the third peak combining finite element computation and experimental characterization of the dynamic mechanical behavior of a model trilayer system. The latter is composed of acrylonitrile butadiene styrene copolymer (ABS) and polycarbonate (PC), two polymers often combined thanks to their complementary properties: heat resistance and toughness of PC (elongation at break at 50 mm/min is 125%) and ease of processability and reliable notched impact resistance of ABS (Charpy notched impact strength at 23°C is 22 kJ/m<sup>2</sup>)<sup>29-31</sup>. ABS and PC are known to be quite compatible since no compatibilizer is needed for ABS/PC blends<sup>32,33</sup>. As shown by some authors, the SAN phase of ABS interacts with the PC, leading to a good adhesion between the two polymers<sup>33-35</sup> and partial miscibility<sup>36</sup>. This trilayer system is therefore of prime interest to consider the effect of an interphase and to determine its effect on the third peak.

## 2. Materials and methods

### 2.1 Materials

Terluran GP 22 Styrolution (BASF) is a very common commercial grade of ABS (MVR = 19 cm<sup>3</sup>/10 min at 220°C with load 10 kg according to ISO 1183 test method) used for this study. Lexan PC 121R is a high fluidity polycarbonate (MFR = 21 cm<sup>3</sup>/10 min at 300°C with load 1.2 kg according to ISO 1183) (SABIC Innovative Plastics). The relative densities and glass transition temperatures of ABS and PC are approximately 1.05 (114°C) and 1.2 (147°C) respectively.

### 2.2 Preparation of blends

Trilayer systems have been realized via thermocompression with a Gibitre hot press (Italy). Films of each polymer have been prepared separately from pellets. First, polymer pellets were dried under vacuum at 80°C for 12h before processing. Then films were pressed in the hot press with a pressure of 100 bars during 30 s at 190°C for ABS and 230°C for PC. The trilayer systems have been obtained by stacking three films (ABS/PC/ABS) and pressing them at 210 °C with a pressure of 100 bars during 3 min. The thicknesses of the three stacked films have been determined in order to get a symmetric ABS/PC/ABS system with relative volume fraction of 70% ABS / 30% PC (denoted respectively  $\phi_{ABS}$ ,  $\phi_{PC}$ ). The total film thickness is comprised between 3 and 4 mm.

## 2.3. Characterization and methods

### 2.3.1 Dynamical rheology

Dynamical Mechanical Thermal Analysis was carried out on small bar samples under nitrogen to avoid polymer degradation and absorption of moisture using a DMTA Q800 from TA Instruments, working in dynamic tensile mode.

Samples were clamped into the DMTA in two different ways (Figure 1): in the “regular” configuration, the layers are parallel to the clamps so that the external layers of the trilayer systems, *i.e.* ABS layers, are in contact with the clamps. In the “orthogonal” configuration, layers are orthogonal to the clamps, so the two polymers are in contact with the clamps.

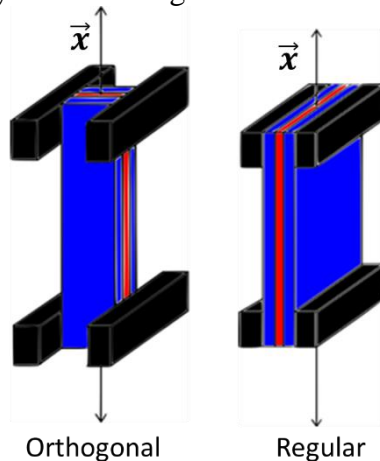


**Figure 1 : Multilayered configurations**

The dimensions of their microstructures are specified in Table 1.

Geometry	$\phi_{PC}$ %	L mm	l mm	h mm	E Mm
Orthogonal	33.5	11.88	5.02	3.42	1.68
Regular	33.3	15.50	3.42	5.02	1.14

**Table 1 : dimensions of the trilayer systems ABS/PC/ABS for the “orthogonal” and “regular” configurations**

An oscillating displacement (in the  $\vec{x}$  direction, corresponding to axial strain  $\epsilon_x$ ) is applied to a sample at a given temperature, and the material response force (in the  $\vec{x}$  direction, corresponding to axial stress  $\sigma_x$ ), corresponding to this displacement, is measured.

The oscillating frequency  $\omega$  was set to 1 Hz, the temperature ( $T$ ) was varied from 25°C to 200°C at 2°C/min heating rate and a strain amplitude ( $\varepsilon_{x0}$ ) of 0.1% was applied during the measurements, which was shown to be in the linear domain both for virgin polymers and blends. For viscoelastic materials, the magnitude of the material response (i.e., the amplitude of force and stress) to the applied oscillating strain is shifted by a phase angle  $\delta$ . From this relation between strain and stress produced in the sample, elastic storage modulus ( $E'$ ) and loss modulus ( $E''$ ) were calculated. All measurements were reproduced twice and were well reproducible. The ratio between  $E''$  and  $E'$  is called damping and is represented as  $\tan \delta$ .

### 2.3.3 Modeling

#### 2.3.3.1 Methodology

Finite element (FE) modeling is an efficient tool to predict material structure properties. Numerical simulations were carried out using FE software ZeBuLon developed at Mines Paristech<sup>37</sup>.

Virgin polymers are expected to follow viscoelastic evolutions. At a first approximation we choose a Maxwell's model using one relaxation time  $\tau_1$  to describe their macroscopic behaviors: considering a multiaxial loading, stress  $\boldsymbol{\sigma}$  and strain  $\boldsymbol{\varepsilon}$  tensors are related by this relation (1):

$$\boldsymbol{\sigma}(t) = \int_0^t 2\mathbf{G}_0 e^{-\frac{t-\tau}{\tau_1}} \dot{\boldsymbol{\varepsilon}}(\tau) d\tau + \mathbf{1} \int_0^t \mathbf{K}_0 e^{-\frac{t-\tau}{\tau_1}} \text{tr}(\dot{\boldsymbol{\varepsilon}}_s) d\tau \quad (1)$$

where the decomposition of  $\boldsymbol{\varepsilon}$  in spherical  $\boldsymbol{e}_s$  and deviatoric  $\boldsymbol{e}$  parts is assumed as Eq. (2):

$$\boldsymbol{\varepsilon}(t) = \boldsymbol{e}_s(t) + \boldsymbol{e}(t), \text{tr}(\boldsymbol{e}(t)) = \mathbf{0}, \boldsymbol{e}_s(t) = \boldsymbol{e}_s \mathbf{1}, \boldsymbol{e}_s \in \mathbb{R} \quad (2)$$

$G_0$  and  $K_0$  are instantaneous shear and bulk moduli. In expression (1) long time shear and bulk modulus are neglected.  $G_0$  and  $K_0$  are related to the Poisson coefficient  $\nu$  via the relation (3):

$$K_0 = -\frac{2}{3} \frac{\nu + 1}{2\nu - 1} G_0 \quad (3)$$

In equations (1) and (2), bold letters refer to tensorial mathematical objects.

In the case of uniaxial oscillatory tensile tests, stress and strain tensors can be expressed as Eq. (4):

$$\boldsymbol{\sigma}(t) = \begin{pmatrix} \sigma_x(t) & 0 & 0 \\ 0 & 0 & 0 \\ 0 & 0 & 0 \end{pmatrix}, \boldsymbol{\varepsilon}(t) = \begin{pmatrix} \varepsilon_x(t) & 0 & 0 \\ 0 & \varepsilon_y(t) & 0 \\ 0 & 0 & \varepsilon_z(t) \end{pmatrix}, \quad (4)$$

where  $\varepsilon_x(t) = \varepsilon_{x0} \sin(\omega t)$ ,  $\varepsilon_y(t)$ ,  $\varepsilon_z(t)$  are the lateral and out of space strains and  $\sigma_x(t) = \sigma_{0x} \sin(\omega t + \delta)$ .

Assuming  $\varepsilon_{x0}$ , material parameters  $\tau_1, \nu$  and  $G_0$  known,  $\sigma_{0x}$  and  $\delta$  can be deduced from a FE simulation. Only one finite element is used for this latest simulation as the simulation corresponds to a homogeneous test and classical boundary conditions of a uniaxial tensile test are applied. As a sinusoidal strain signal (amplitude  $\varepsilon_{x0}$ , frequency  $\omega$ ) is applied, the analysis of stress signal after numerical simulation enables the determination of  $\sigma_{0x}$  and  $\delta$ .

#### 2.3.3.2 Identification of material parameters of virgin polymers

DMTA experiments are able to evaluate the evolution of  $E'(T)$ ,  $E''(T)$  and thus  $\tan \delta(T)$  versus temperature for neat polymers.

From  $\delta(T)$  and  $E'(T)$ , the evaluation of stress magnitude  $\sigma_{0x}$  is available for each testing temperature via the relation (5):

$$\sigma_{0x}(T) = \frac{\varepsilon_{0x} E'(T)}{\cos \delta(T)} \quad (5)$$

As rheological behavior of each polymer is strongly dependent of temperature, it is assumed by that way that virgin polymer behavior can be described via the knowledge of three parameters  $\tau_1, \nu$  and  $G_0$ , strongly dependent on temperature.

The optimum material parameters  $(\tau_1, \nu, G_0)$  correspond to the best accordance between experimental and numerical strain amplitude and phase shift.

To solve this non-linear problem, an optimization scheme, based on Sequential Quadratic Programming (SQP) algorithm, is selected. This second order local optimizer is included in the optimisation module “Z-optim” of ZeBuLon’s software. The gap between experimental and numerical stress values  $\sigma_{0x}$  and  $\delta$  at each temperature  $T$  is computed via a cost function written as follows:

$$J(\tau_1, \nu, G_0) = \frac{1}{2} (\sigma_{0x}(\tau_1, \nu, G_0) - \sigma_{0x \text{ exp}})^2 + (\delta(\tau_1, \nu, G_0) - \delta_{\text{exp}})^2 \quad (6)$$

The problem is thus to solve, at each temperature following Eq. (7):

$$\text{Inf}_{(\tau_1, \nu, G_0) \in \mathbb{R}^3} J(\tau_1, \nu, G_0) \quad (7)$$

### 2.3.3.3 Prediction of multilayered behavior

A quarter of the geometry of the trilayer model system is considered thanks to the symmetries of the geometry and boundary conditions Geometry and meshes are presented in **Erreur ! Source du renvoi introuvable.** In FE simulations displacement continuity is assumed at the interface ABS/PC. Materials properties of ABS and PC, for each temperature, are defined through preliminary simulations (see part 2.3.3.2). The volumes are subjected to displacement values  $h\varepsilon_{0x} \sin(\omega t)$  on lateral surfaces delimited by the dotted rectangle (height of 2 mm) on **Figure 2**.  $E'(T)$ ,  $E''(T)$  and thus  $\tan \delta(T)$  of the multilayered materials can therefore be obtained and compared to the experimental ones.

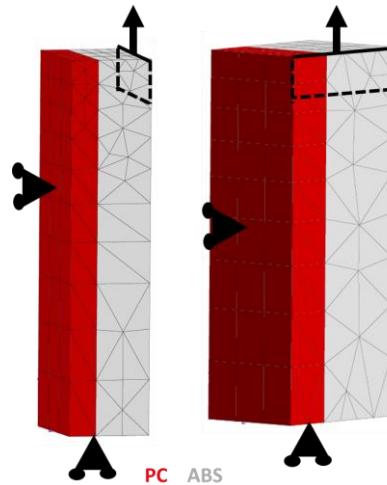


Figure 2 : FE geometries and meshes, “regular” (left) “orthogonal” (right) configuration

## 3. Results and discussion

### 3.1. Rheological properties

#### 3.1.1 Virgin polymers

Figure 3 presents the evolution of  $E'$  and  $\tan \delta$  as a function of temperature for ABS and PC polymers obtained with DMTA equipment. Both polymers exhibit one transition peak corresponding to the glass transition temperature of the amorphous polymers, located at 114°C and 147°C for ABS and PC respectively. As expected, the storage moduli show a pronounced decrease of two to three decades after the glass transitions.

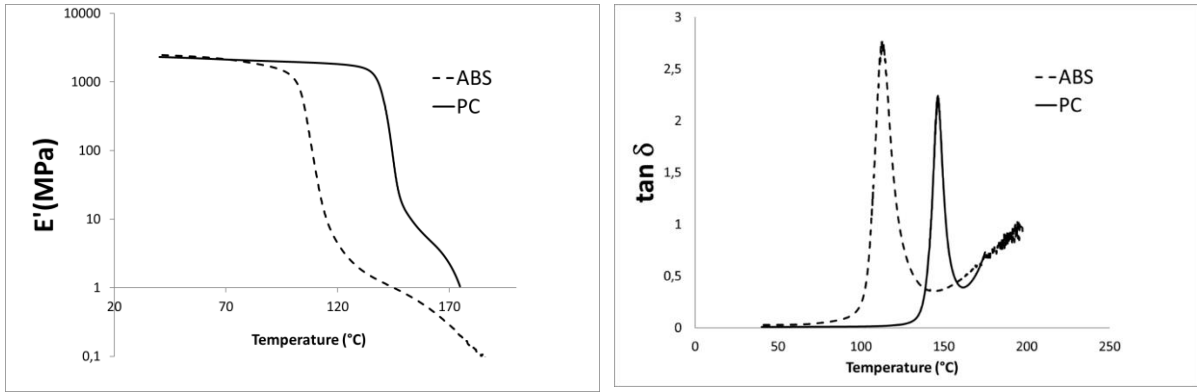


**Figure 3 : Evolution of storage moduli (left) and loss tangent moduli (right) of neat polymer ABS and PC versus temperature**

### 3.1.2 Multilayered structure behaviour

Results of the dynamic mechanical analysis of the multilayered materials are presented in Figure 4. In both “orthogonal” and “regular” configurations, native damping peaks of PC and ABS are visible, which is clearly an indication of PC and ABS immiscibility. As expected, the storage modulus decreases with temperature for both configurations while shifted for the “orthogonal” configuration.

Moreover the “regular” multilayer structure leads to the presence of an additional intermediate damping peak. As discussed in the introduction, the origin of this intermediate peak is still debated. The fact that this third peak is measured only for “regular” configuration would suggest that its origin is rather purely mechanical and reflects the additive effect of the damping behavior of ABS and PC. Moreover, the contribution of the residual stresses<sup>38</sup> and their progressive relaxation in temperature should be involved. Modelling approach was used to shed new light on the origin of this peak.

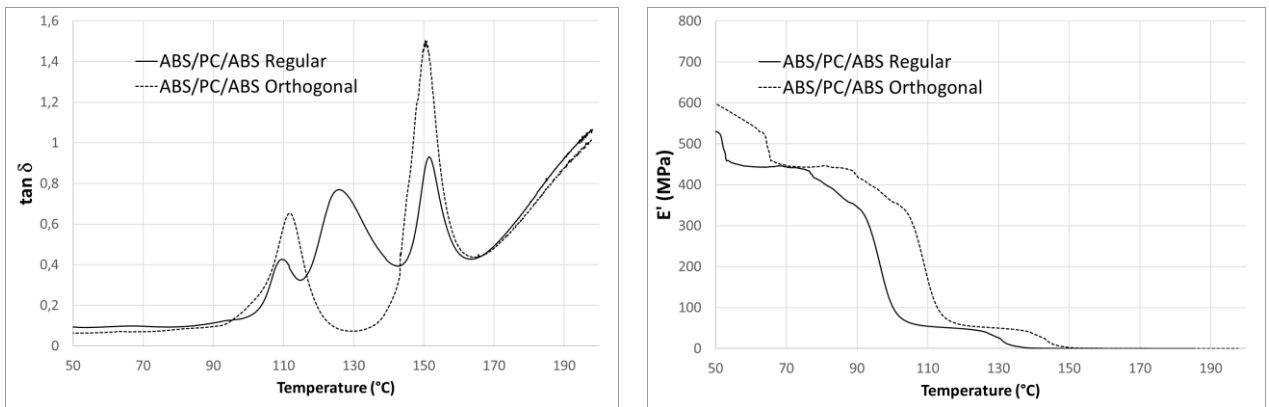


**Figure 4 : Effect of the orientation of the sample in DMTA apparatus on the intermediate peak (left) and on the storage modulus (right) for ABS/PC/ABS three-layer samples**

## 3.2 Modelling

### 3.2.1 Virgin polymers

The first step was to define materials properties ( $\tau_1, \nu, G_0$ ) of ABS and PC depending on temperatures. The methodology used is the one presented in part 2.3.3.2. The discrete temperatures are chosen to correspond to critical points of  $E'(T)$  and  $\tan \delta(T)$ :

$T \in \{100, 108, 110, 113, 117, 120, 125, 130, 135, 140, 143, 147, 150, 155, 160\}^\circ\text{C}$ .

The Poisson’s ratio of viscoelastic materials cannot be regarded as a constant parameter, but as a time-dependent material function, being increased according to the temperature. Some authors

found that this dependence can be fitted with a sigmoidal function, extending from a lower plateau value to an upper plateau value scattered around 0.5<sup>39,40</sup>. For the sake of simplicity, we assume a bilinear evolution for the Poisson's ratio from the value given in the data sheet ( $\nu_{PC} = 0.37$ ,  $\nu_{ABS} = 0.42$  at 25°C) to 0.5 around glass transition (see Figure 5).

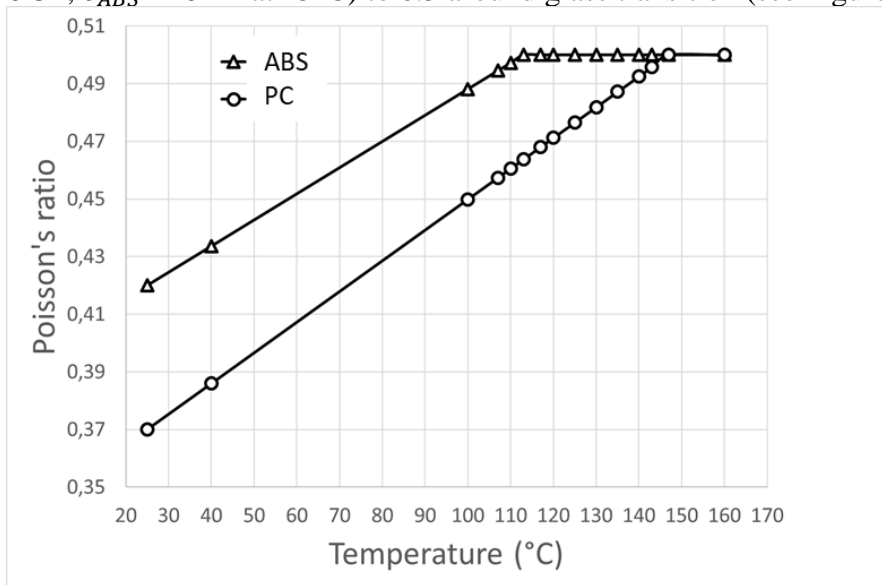


Figure 5 : Poisson's ratio of PC and ABC versus temperature– trend curves (solid line)

The algorithm of minimization quickly converges towards a solution for each polymer and each temperature.  $(\tau_1, G_0)$  are presented in Figure 6 and Figure 7 (left) for the temperatures between 100 to 160°C, stages of maximum variabilities for these variables. These material parameters lead to an accurate description of  $\tan \delta(T)$  curve (see dot points corresponding to this minimization on the graph of Figure 7 (right)).

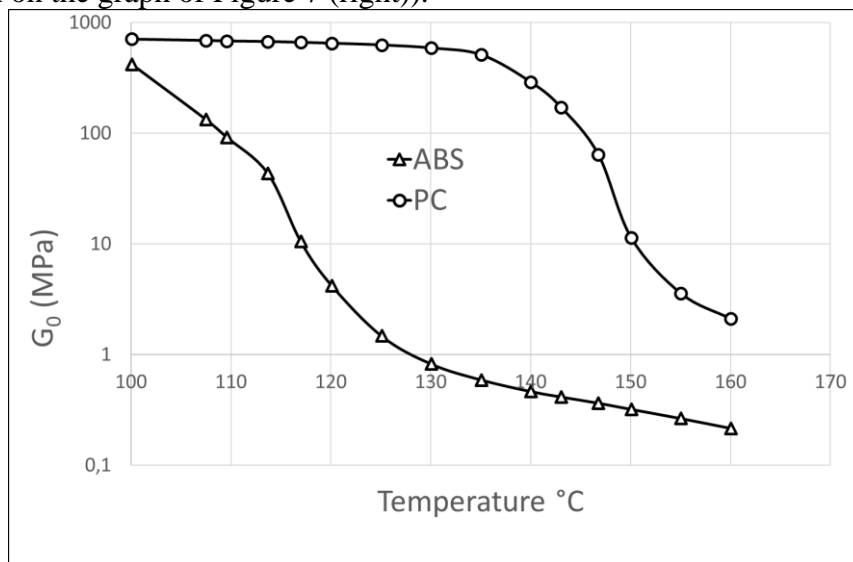
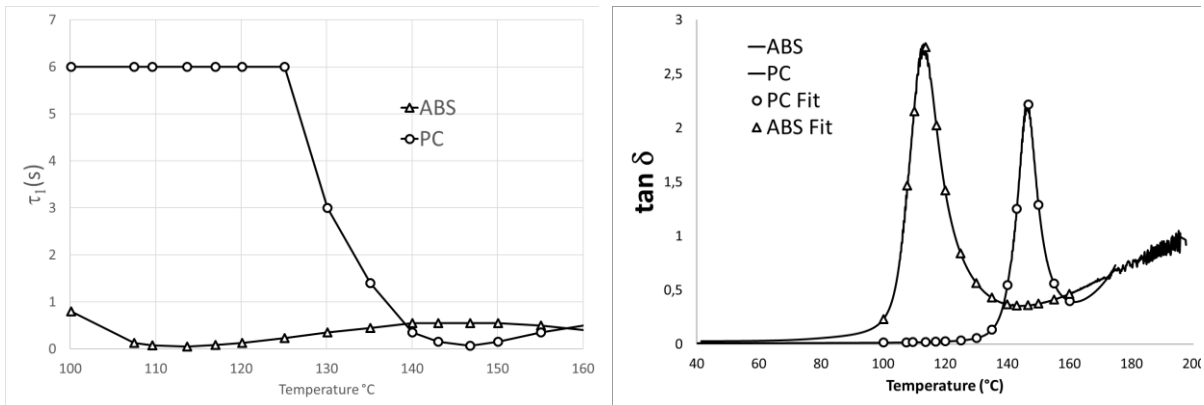


Figure 6 : Instantaneous shear modulus versus temperature – zoom on temperatures between 100 to 160°C– trend curves (solid line)





**Figure 7 : Relaxation time versus temperature of virgin polymers ABS and PC – zoom on temperatures between 100 to 160°C (left) Discrete fitting of  $\tan \delta(T)$  of ABS (triangles) and PC (circles) (right) – trend curves (solid line)**

### 3.2.2 Multilayered materials

Numerical computations are conducted through 3D simulations as described in section 2.3.3.2. Comparison between loss factors related to “orthogonal” and “regular” loadings is given in Figure 8. As expected, the loss factor peaks of native polymers are clearly present even if for the “orthogonal” simulation, the one of ABS is slightly shifted towards the lower temperatures. Moreover, for the “regular” configuration, ABS layer does not transmit the load as it shows a low elastic modulus, in comparison to PC. In both configurations, layers are not subjected to the same level and nature of stress. This observation is not sufficient to explain the apparition of the additional third peak.

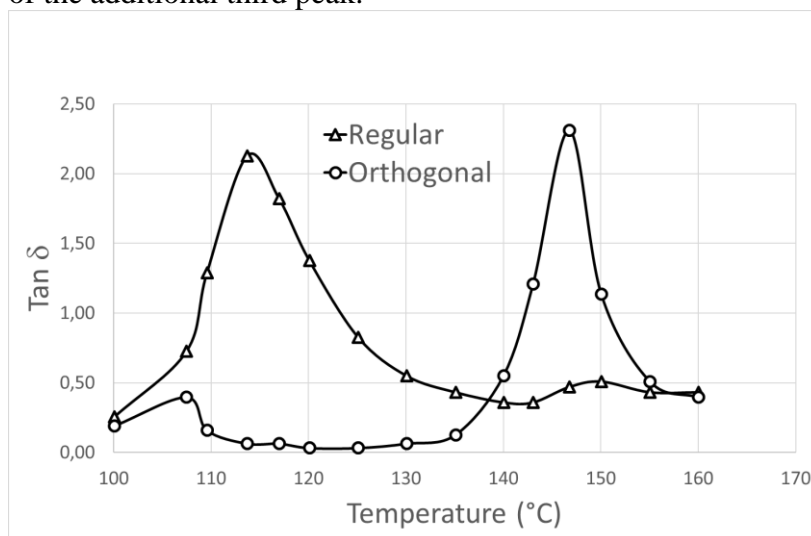


**Figure 8 : Loss factors versus temperature for multilayered structures ABS/PC/ABS “orthogonal” and “regular” – zoom on temperatures between 100 to 160°C– trend curves (solid line)**

### 3.3 Discussion

#### 3.3.1 Predictive simulation with an interphase

To go further, the hypothesis of an interphase between ABS and PC is investigated using the numerical simulation, as Patel et al. have done it for nanocomposites materials<sup>41</sup>. To do so, an interphase with material average properties mainly due to the possible SAN-PC miscibility was considered. An interphase with an arbitrary thickness of 0.4 mm is assumed between ABS and PC considering the partial ABS-PC miscibility of a 25 wt% SAN rate.

The dimensions of the new microstructures are specified in Table 2. As the interphase size has been arbitrarily fixed, a sensitivity analysis is then conducted.

Geometry	$\phi_{PC}$ %	L mm	l mm	h mm	e mm	i mm
Orthogonal	33.5	11.88	5.02	3.42	1.48	0.4
Regular	33.3	15.50	3.42	5.02	0.94	0.4

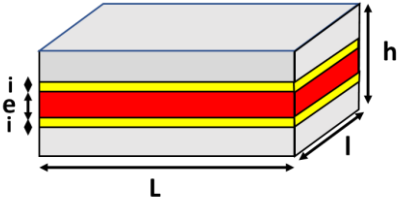


**Table 2 : Multilayered dimensions for “orthogonal” and “regular” microstructures ABS/PC/ABS assuming the existence of an interphase**

We use the Fox’s equation<sup>42</sup> to predict the interphase damping peak ( $T_{g\ inter}$ ) from the one of native polymers ( $T_{g\ PC}, T_{g\ ABS}$ ). As we assume miscibility in the interphase area, the interphase damping factor can be deduced from:

$$\frac{1}{T_{g\ inter}} = \frac{\phi_{PC}}{T_{g\ PC}} + \frac{1-\phi_{PC}}{T_{g\ ABS}} \quad (8)$$

$T_{g\ inter}$  was estimated around 123°C.

The same methodology as the one proposed for the virgin polymer is used to define materials properties ( $\tau_{inter}, \nu_{inter}, G_{inter}$ ) of this interphase. A set of parameters for this interphase:  $G_{0\ inter} = G_{0\ ABS}, \nu_{inter} = \nu_{ABS}$  and  $\tau_{inter}$  leads to a good representation of the interphase relaxation. This relaxation time of the interphase is presented in Figure 9 (left) in comparison with native polymers. This interphase exhibits a maximum peak in its loss factor at 123°C; below and above this value, the behavior interphase is between native polymers (Figure 9 (right)).

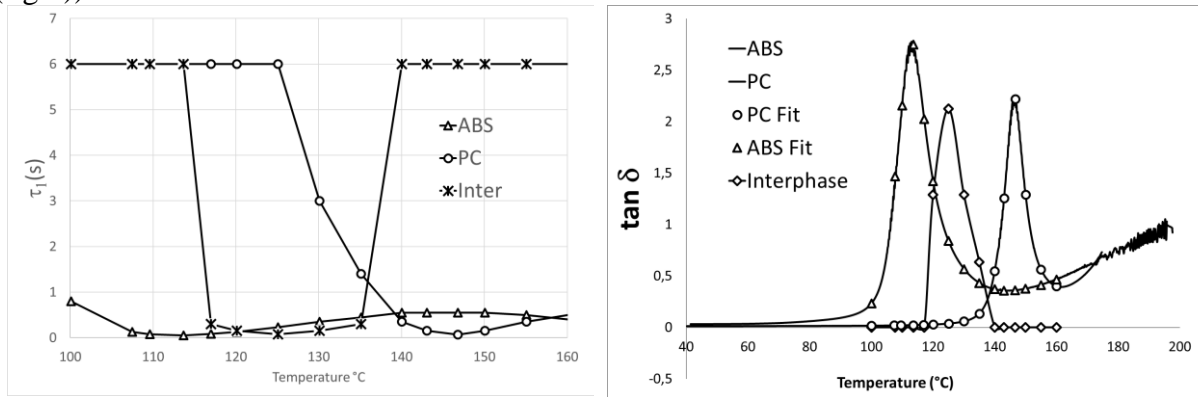


**Figure 9 : Relaxation time versus temperatures of interphase and virgin polymers ABS, PC – zoom on temperatures between 100 to 160°C – trend curves (solid line) (left) Evolution of  $\tan \delta(T)$  (continuous line) versus time and discrete fitting (diamond) of interphase behaviour (right)**

A predictive modelling is conducted using these new microstructures; the geometries and meshes are given in Figure 10 (left); boundary conditions are those described in part 2.3.3.3. Results of the finite element simulations are given in Figure 10 (right) for “orthogonal” and “regular” configurations. For the “orthogonal” sample, the presence of the interphase does not impact the evolution of  $\tan \delta$ . For the “regular” configuration, the interphase conducts to an increase of  $\tan \delta$  between the damping peaks of ABS and PC. This increase could be related to the additional peak observed in the experimental value obtained for the “regular” multilayered sample (Figure 4). To go further in this analysis, the interphase behaviour should be finely characterized with microscopy tools (e.g. AFM for example).

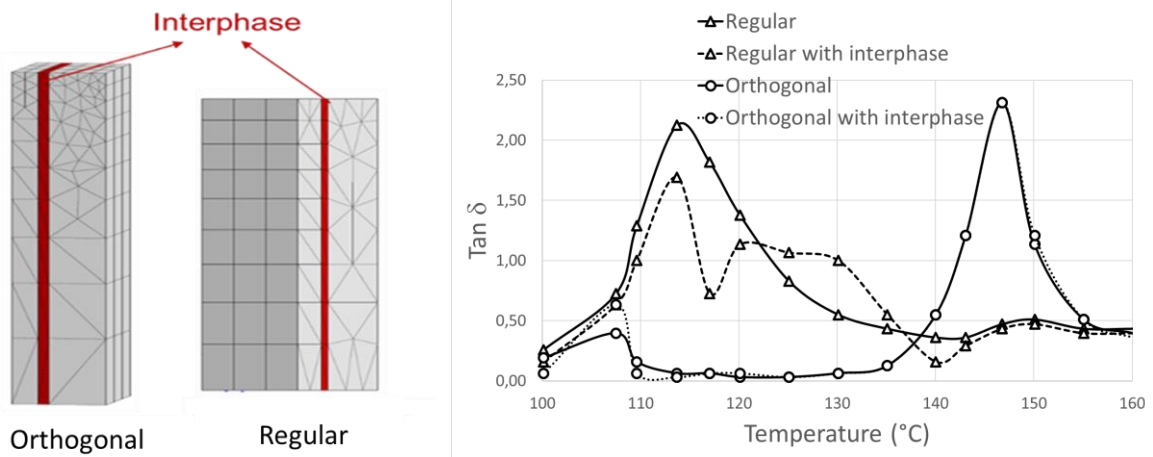


**Figure 10 : FE geometries and meshes for multilayered materials ABS/PC/ABS with interphase between layers (left) Loss factors versus temperature for multilayered ABS/PC/ABS structures “orthogonal” and “regular” with an interphase of 0.4 mm between the layers – zoom on temperatures between 100 to 160°C (right)**

The charge transfer in the multilayered material is very different in the presence of the interface between the two configurations. The average strain components can be numerically evaluated in both situations for each layer component (ABS, PC and interphase).

An equivalent strain can be computed as follow (Eq. 9):

$$\varepsilon_{eq} = \frac{1}{\sqrt{2}} \left[ (\varepsilon_{xx} - \varepsilon_{yy})^2 + (\varepsilon_{yy} - \varepsilon_{zz})^2 + (\varepsilon_{zz} - \varepsilon_{xx})^2 + 6(\varepsilon_{xy}^2 + \varepsilon_{xz}^2 + \varepsilon_{yz}^2) \right]^{1/2} \quad (9)$$

This equivalent average strain is given in Figure 11 for samples loaded under a temperature of 125°C and for an axial strain of 0.04%. It appears that in the “regular” configuration the PC layer is almost not loaded, which leads to a disappearance of its associated peak at 147°C in Figure 10. On the other hand, the interphase in the “regular” configuration exhibits the higher equivalent strain (0.1%), which could explain the increase of the loss damping between the two native peaks of PC and ABS. In the “orthogonal” configuration, the equivalent strain is almost the same for all layers of the components, suggesting that the interphase is not sufficiently stretched to contribute to the loss factor evolution.

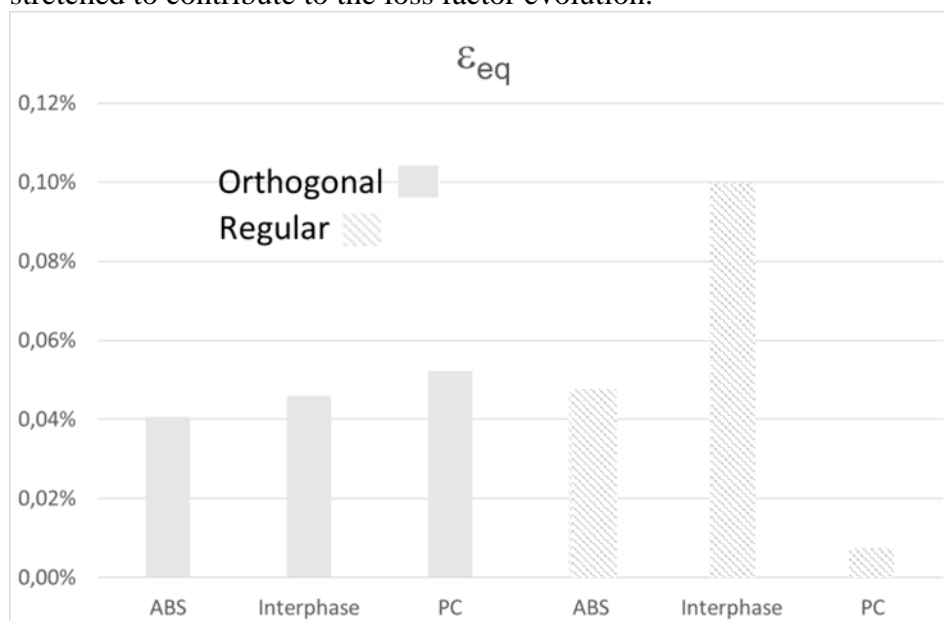


**Figure 11 : Average value of the equivalent strain in each layer of material for “orthogonal” and “regular” ABS/PC/ABS configuration at 125°C and for an applied axial strain of  $4 \times 10^{-4}$**

### 3.3.2 Sensitivity analysis

Further analyzes are needed to properly describe the interphase between layers. Let us first consider the thickness of the interface, value which was fixed a priori in the previous study. As it is shown in Figure 12 (left), decreasing the thickness of the interface leads to lessen the contribution of the interphase (by decreasing the value of  $\tan \delta$  between 120°C to 130°C) to favor that of ABS (at 114°C).

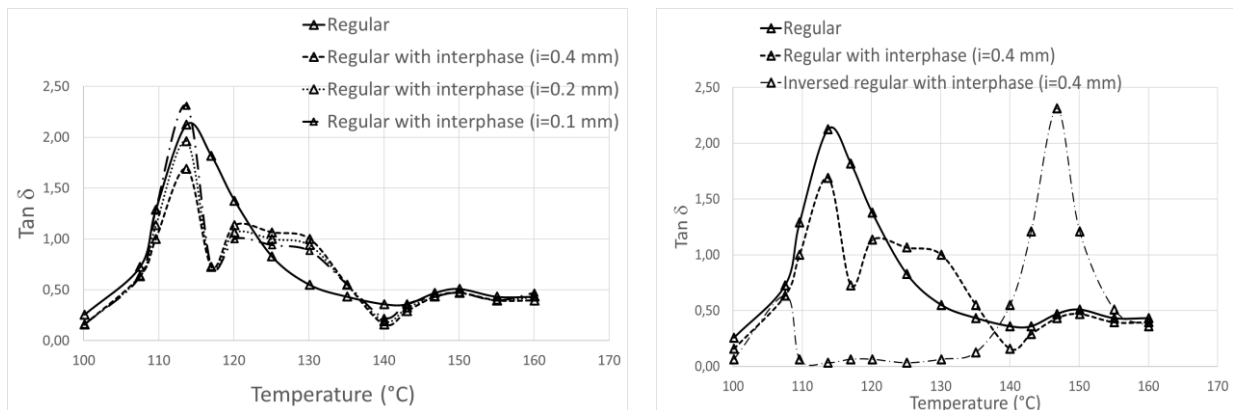


**Figure 12 : Loss factors versus temperature: for “regular” (ABS/PC/ABS) (left) ; for “inverse regular”(PC/ABS/PC) multilayered structure with 0.4 mm interphase» (right) – zoom on temperatures between 100 to 160°C**

## Conclusion

Trilayer ABS/PC/ABS films fabricated by thermocompression have been characterized using dynamic mechanical thermal analysis in tensile mode. When the film is loaded in parallel to the layers, an intermediate damping peak is observed in the DMTA curves, while this peak is not present when the film is loaded orthogonally to the layers. Numerical computations show no difference in the behavior of the films in both configurations, suggesting that the origin of the observed intermediate peak is not a purely mechanical phenomenon. However, assuming the presence of an interphase with its own behavior and thickness leads to differences in the local mechanical behavior of the two configurations. Moreover, computations reveal the appearance of an additional peak for the loss factor as the film is loaded in parallel to its layers. The interphase thickness considered in the computations (around 400  $\mu\text{m}$ ) seems in reasonable accordance with interphases measured for compatible polymer blends. More experiments are needed to properly quantify and qualify this interphase, but this first study shows clearly the relevance of an interphase. Dynamic tests Charpy, Izod or dynamic traction could confirm this conclusion. Since polycarbonate is more notch sensitive than ABS, the “regular” sample direction should allow more absorption of impact energy (due to the presence extra peak) in comparison with the “orthogonal” one.

## References

1. 'Boudenne A, 'Ibos, L 'Candau, Y 'Thomas, S. *Handbook of Multiphase Polymer Systems*. (John Wiley and Sons Ltd, ed.); 2011.
2. Pukánszky B. Interfaces and interphases in multicomponent materials: past, present,

- future. *Eur Polym J.* 2005;41(4):645-662. doi:10.1016/J.EURPOLYMJ.2004.10.035
3. Zamani Zakaria A, Shelesh-Nezhad K. The Effects of Interphase and Interface Characteristics on the Tensile Behaviour of POM/CaCO<sub>3</sub> Nanocomposites. *Nanometerials Nanotechnol.* 2014;4.
  4. Chen GX, Kim HS, Park BH, Yoon JS. Multi-walled carbon nanotubes reinforced nylon 6 composites. *Polymer (Guildf).* 2006;47(13):4760-4767. doi:10.1016/j.polymer.2006.04.020
  5. Zare Y, Rhee KY. Accounting the reinforcing efficiency and percolating role of interphase regions in tensile modulus of polymer/CNT nanocomposites. *Eur Polym J.* 2017;87:389-397. doi:10.1016/j.eurpolymj.2017.01.007
  6. Qi W, Liu M, Wu J, et al. Promoting the thermal transport via understanding the intrinsic relation between thermal conductivity and interfacial contact probability in the polymeric composites with hybrid fillers. *Compos Part B Eng.* 2022;232(January):109613. doi:10.1016/j.compositesb.2022.109613
  7. Zid S, Zinet M, Espuche E. Modeling diffusion mass transport in multiphase polymer systems for gas barrier applications: A review. *J Polym Sci Part B Polym Phys.* 2018;56(8):621-639. doi:10.1002/polb.24574
  8. Colin X, Teyssède G, Fois M. Ageing and degradation of multiphase polymer systems. In: Boudenne A, Ibos L, Candau Y, Thomas S, eds. *Handbook of Multiphase Polymer Systems.* John Wiley. ; 2011:797-841.
  9. Koriyama H, Oyama HT, Ougizawa T, Inoue T, Weber M, Koch E. Koriyama 1999. copolymer and PApdf. 1999;40:6381-6393.
  10. Zhang J, Lodge T, Macosko C. Interfacial morphology development during PS/PMMA reactive coupling. *Macromolecules.* 2005;38:6586-6591.
  11. Stamm M, Schubert DW. Interfaces Between Incompatible Polymers. *Annu Rev Mater Sci.* 1995;25:325-356.
  12. Cavaillé J, Jourdan C, Perez J. Dynamic Mechanical Spectrometry for the Study of Multiphase Polymer Materials. *Makromol Chemie Macromol Symp.* 1988;16:341-360.
  13. Cavaillé J, Perez J. Polymer Physics and Characterization by Mechanical Measurements. *Makromol Chemie Macromol Symp.* 1990;35:405-422.
  14. Lewis TB, Nielsen LE, Company M. Dynamic Mechanical Properties of Particulate-Filled Composites. 1970;14:1449-1471.
  15. Eklind H, Schantz S, Maurer FHJ, Jannasch P, Bengt W. Characterization of the interphase in PPO/PMMA blends compatibilized by P(S-g-EO). *Macromolecules.* 1996;29:984-992.
  16. Douglas EP, Waddon AJ, MacKnight WJ. Viscoelastic and Morphological Study of Ionic Aggregates in Ionomers and Ionomer Blends. *Macromolecules.* 1994;27(15):4344-4352. doi:10.1021/ma00093a040
  17. Girard-Reydet E, Sautereau H, Pascault JP. Use of block copolymers to control the morphologies and properties of thermoplastic/thermoset blends. *Polymer (Guildf).* 1999;40(7):1677-1687. doi:10.1016/S0032-3861(98)00302-4
  18. Eklind H, Maurer FHJ. Micromechanical transitions in compatibilized polymer blends. *Polymer (Guildf).* 1996;37(13):2641-2651. doi:10.1016/0032-3861(96)87623-3
  19. Colombini D, Maurer FHJ. Origin of additional mechanical transitions in multicomponent polymeric materials. *Macromolecules.* 2002;35(15):5891-5902. doi:10.1021/ma020266l
  20. Gregory B, Hiltner A, Baer E, Im J. Dynamic mechanical behavior of continuous multilayer composites. *Polym Eng Sci.* 1987;27(8):568-572. doi:10.1002/pen.760270807
  21. McLaughlin KW. The influence of microstructure on the dynamic mechanical behavior

- of polycarbonate/poly(styrene - co - acrylonitrile) blends. *Polym Eng Sci.* 1989;29(22):1560-1568. doi:10.1002/pen.760292203
22. Nazarenko S, Haderski D, Hiltner A, Baer E. Origin of the intermediate damping peak in microlayer composites. *Polym Eng Sci.* 1995;35(21):1682-1687. doi:10.1002/pen.760352104
  23. Hsieh AJ, Gutierrez AW. Thermal Characterization of a Microlayered Polycarbonate/Polymethyl Methacrylate Composite. *MRS Online Proc Libr.* 1996;461:165-171.
  24. Shen J, Li J, Guo S. The origin of a new transition in dynamic mechanical spectra of multilayer polymeric composite. *Polymer (Guildf).* 2012;53(12):2519-2523. doi:10.1016/j.polymer.2012.04.004
  25. Shen J, Wang M, Li J, et al. Simulation of mechanical properties of multilayered propylene-ethylene copolymer/ethylene 1-octene copolymer composites by equivalent box model and its experimental verification. *Eur Polym J.* 2009;45(11):3269-3281. doi:10.1016/j.eurpolymj.2009.07.013
  26. Zhang F, He G, Xu K, Wu H, Guo S. The damping and flame-retardant properties of poly(vinyl chloride)/ chlorinated butyl rubber multilayered composites. *J Appl Polym Sci.* 2015;132(2):1-7. doi:10.1002/app.41259
  27. Chua PS. Dynamic mechanical analysis studies of the interphase. *Polym Compos.* 1987;8(5):308-313. doi:10.1002/pc.750080505
  28. Zhang F, Guo M, Xu K, He G, Wu H, Guo S. Multilayered damping composites with damping layer/constraining layer prepared by a novel method. *Compos Sci Technol.* 2014;101:167-172. doi:10.1016/j.compscitech.2014.06.021
  29. Greco R. "Natural" Polymer Alloys: PC/ABS Systems. In: *Polymer Blends and Alloys.* ; 2019:289-330.
  30. Roberto G, Sorrentino A. Polycarbonate/ABS blends: A literature review. *Adv Polym Technol.* 1994;13:249-258.
  31. Suarez H, Barlow J, Paul D. Mechanical Properties of ABS/Polycarbonate Blends. *J Appl Polym Sci.* 1984;29(11):3253-3259.
  32. Guinault ACS. Thermomechanical properties of ABS/PA and ABS/PC blends. *Int J Mater Form.* 2009;2(1):701-704.
  33. Keitz JD, Barlow JW, Paul DR. Polycarbonate blends with styrene/acrylonitrile copolymers. *J Appl Polym Sci.* 1984;29(10):3131-3145. doi:10.1002/app.1984.070291016
  34. Carrasco F, Santana O, Cailloux J, Sanchez-Soto M, MasPOCH ML. Poly(lactic acid) and acrylonitrile-butadiene-styrene blends: influence of adding ABS-g-MAH compatibilizer on the kinetics of the thermal degradation. *Polym Test.* 2018;67:468-476.
  35. Kim WN, Burns CM. Phase behavior of blends of polycarbonate with partially miscible polymers. *J Appl Polym Sci.* 1990;41(7-8):1575-1593. doi:10.1002/app.1990.070410718
  36. Aid S, Eddhahak A, Ortega Z, Froelich D, Tcharkhtchi A. Experimental study of the miscibility of ABS/PC polymer blends and investigation of the processing effect. *J Appl Polym Sci.* 2017;134:44975.
  37. Besson, J.; Leriche, R.; Foerch, R.; Cailletaud G. Object-oriented programming applied to the finite element method Part II. application to material behaviors. *Rev Eur des Éléments Finis.* 1998;7:567-588.
  38. Akay M, Ozden S. Influence of residual stresses on mechanical and thermal properties of injection moulded polycarbonate. *Plast Rubber Compos Process Appl.* 1996;25(3):138-144.

39. Pandini S, Pegoretti A. Time and temperature effects on Poisson's ratio of poly(butylene terephthalate). *Express Polym Lett.* 2011;5(8):685-697.
40. Yang L, Yang L, Lowe RL. A viscoelasticity model for polymers: Time, temperature, and hydrostatic pressure dependent Young's modulus and Poisson's ratio across transition temperatures and pressures. *Mech Mater.* 2021;157(August 2020):103839. doi:10.1016/j.mechmat.2021.103839
41. Patel RK, Bhattacharya B, Basu S. Effect of interphase properties on the damping response of polymer nano-composites. *Mech Res Commun.* 2008;35(1-2):115-125. doi:10.1016/j.mechrescom.2007.08.005
42. Fox TG. Influence of Diluent and of Copolymer Com- position on the Glass Temperature of a Polymer System. *Bull Am Phys Soc.* 1956;1:123.